Nuclear Materials and Energy 26 (2021) 100933

Contents lists available at ScienceDirect

Nuclear Materials and Energy

journal homepage: www.elsevier.com/locate/nme

Impact of the new TCV baffled divertor upgrade on pedestal structure and performance

U.A. Sheikh [a,*], M. Dunne [b], L. Frassinetti [c], B. Labit [a], P. Blanchard [b], B.P. Duval [a], O. Février [a], D. Galassi [a], A. Merle [a], H. Reimerdes [a], C. Theiler [a], the TCV Team [1], the EUROfusion MST1 Team [2]

[a] École Polytechnique Fédérale de Lausanne (EPFL), Swiss Plasma Center (SPC), CH-1015, Lausanne, Switzerland
[b] Max-Planck-Institut fur Plasmaphysik, 85748 Garching b. Munchen, Germany
[c] KTH Royal Institute of Technology, Stockholm, Sweden

ARTICLE INFO

Keywords:
Pedestal
Baffles
TCV

ABSTRACT

A new set of carbon tiles, neutral beam heating optics and gas baffles were installed on TCV during the baffled divertor upgrade in early 2019. The installation of the baffles allows a deconvolution of the roles of main chamber and divertor neutral pressure on the H-mode pedestal structure. This physical barrier allows relatively high neutral pressures to be constrained to the divertor, thus preventing neutrals from entering the main chamber and potentially degrading core confinement. This study presents the experimentally measured and modelled pedestal heights and structure for a series of H-mode discharges prior to and after this upgrade.

Increased pedestal performance at high divertor neutral pressure was observed after the baffled divertor upgrade. This was consistent across all triangularities and outer target locations investigated and is attributed to higher pedestal top temperatures being maintained at high gas injection rates. ASTRA simulations indicated beam heating power coupled to the plasma did not significantly vary after the baffled divertor upgrade or as a function of divertor neutral gas pressure. Analysis of the pedestal structure exposed a strong correlation between pedestal performance and the density pedestal position prior to and after the baffled divertor upgrade. The baffled divertor upgrade limited the outward shift of the density pedestal, thus maintaining higher pedestal performance at high divertor neutral pressures. Stability analysis indicated the majority of discharges studied were within 25% of the stability boundary. No correlation was found between the distance from the stability boundary and pedestal performance or structure. Comparison with the EPED1 model indicated that TCV discharges do not have a fixed dependence between pedestal β_θ and pedestal width. A large variation in the EPED1 relating parameter was observed and found to vary with the density pedestal position.

1. Introduction

The high confinement plasma mode (H-mode) is defined by an edge transport barrier that produces strong temperature and density gradients termed the pedestal [1]. This operational mode produces the highest performance discharges and it is currently foreseen that next step fusion devices will operate in H-mode with a detached divertor. Access to detachment is primarily achieved through additional fuelling and puffing of impurities and this can have a significant influence on the pedestal, which has been shown to be strongly linked to fusion yield [2].

Experiments on ASDEX Upgrade (AUG), JET and unbaffled TCV have shown that increased fuelling can reduce pedestal performance. Analysis of AUG discharges showed a change in the high field side high density (HFSHD) region, which led to an outward shift in pedestal position, degrading the pedestal stability [3–5]. No definitive explanation has yet been produced for JET and TCV but a correlation with the relative shift in temperature and density pedestal positions has been reported [6–9].

An understanding of the structure of the pedestal is given in terms of the EPED framework [10]: the pedestal gradient is set by a transport limit (often taken to be a kinetic ballooning mode (KBM) or similar proxy) while the combination of the gradient and pedestal width (ultimately, the pedestal height) is determined by the onset of a global peeling–ballooning mode (triggering an ELM crash). A characteristic pedestal cycle begins with a steepening pressure gradient until a maximum limit is reached. This limit is dictated by transport and modelled

* Corresponding author.
E-mail address: umar.sheikh@epfl.ch (U.A. Sheikh).
[1] See the author list of S. Coda et al., 2019 *Nucl. Fusion* **59** 112023.
[2] See the author list of B. Labit et al., 2019 *Nucl. Fusion* **59** 086020.

https://doi.org/10.1016/j.nme.2021.100933
Received 3 August 2020; Received in revised form 21 January 2021; Accepted 26 January 2021
Available online 27 January 2021

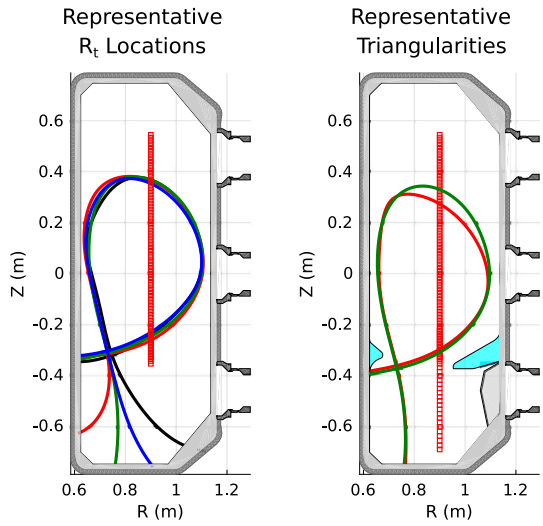

Fig. 1. Left — Unbaffled TCV configuration with representative R_t locations. Thomson scattering measurement locations shown in red squares. Right — Baffled TCV configuration with two representative triangularities. Additional divertor Thomson scattering locations were installed with the baffles. (For interpretation of the references to colour in this figure legend, the reader is referred to the web version of this article.)

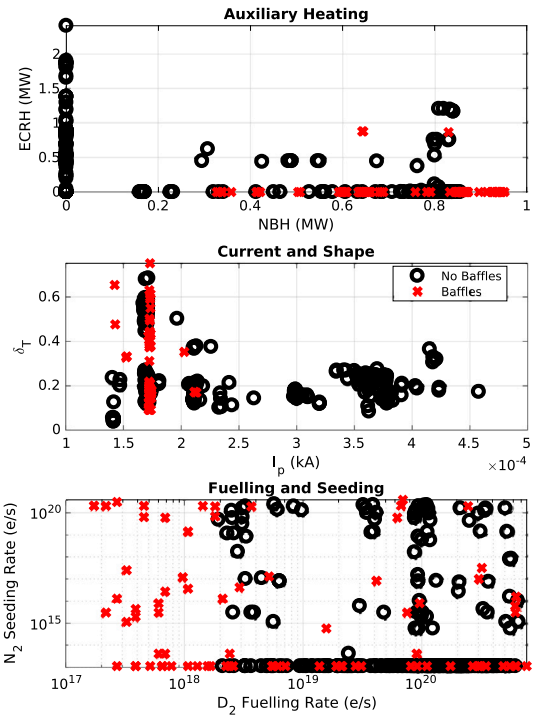

Fig. 2. Overview of discharges analysed. Top — Injected auxiliary heating power, middle — upper triangularity and plasma current, bottom — nitrogen seeding and fuelling rates.

using KBM stability as a proxy. The pedestal width then increases at the maximum gradient until the PB stability boundary. The gradient limit can be inverted to a relation between the pedestal height and width (w) to give the well known dependence with pedestal poloidal β ($\beta_\theta^{Ped.}$): $w = D\sqrt{\beta_\theta^{Ped.}}$. The parameter D relates to the pedestal gradient and thus to the transport [10].

In early 2019, TCV was fitted with new graphite tiles, improved neutral beam heating (NBH) optics and a baffled divertor. The NBH optics were designed increase NBH power into the plasma chamber by 10% through a reduction in beam duct losses. To simplify the comparison between the discharges prior to and after the upgrade, the presented NBH power is the total beam power entering the main plasma chamber (total NBH power minus beam duct losses). The introduction of baffles is expected to significantly reduce the neutral population at the edge of the plasma [11,12]. This in turn is expected to influence the turbulence dominated transport at the plasma edge, which can significantly alter pedestal performance [8,10]. Investigation of transport through the D parameter from the EPED1 model allows for comparisons with unbaffled discharges and a decoupling of the roles of main chamber and divertor neutral pressure on the H-mode pedestal structure.

2. Experiment description

TCV is a carbon walled machine with strong shaping capabilities and a recently installed divertor baffle [11,13,14]. Stationary ELM-y H-mode discharges have been achieved in Ohmic only scenarios and with auxiliary heating through NBH and/or electron cyclotron resonance heating (ECRH). Standard gas injection is from the divertor floor and this was maintained in all discharges presented in this study. A high resolution Thomson scattering system is used to measure T_e and n_e at the locations indicated by red squares in Fig. 1. A high spatial resolution region near the separatrix is equipped with filters optimised for lower T_e measurements (down to 10 eV), providing enhanced measurements of the pedestal [15].

The Thomson scattering system uses three lasers with a pulse rate of 50 ms providing profiles every ~17 ms in standard operation. The lasers can be operated in burst mode, allowing for three profiles in 3 ms with a 50 ms delay between bursts and this mode of operation is preferred during ELM-y H-mode plasmas. All measurements obtained within the last 30% of the ELM cycle are combined and fitted with an mtanh function as described in [16,17]. The profiles are radially shifted such that the seperatirx temperature is set to 50 eV, a value obtained from previous TCV database scaling [18].

Table 1
Ranges of no/low, medium or high fuelling and seeding rates.

	Fuelling	Seeding
No/Low (e/s)	$<10^{19}$	0
Medium (e/s)	10^{19}–10^{20}	10^{13}–10^{18}
High (e/s)	$>10^{20}$	$>10^{18}$

3. Results

A total of 364 H-mode discharges carried out in the MST-1 campaign since the installation of the NBH system on TCV were investigated in this study [19]. They were analyses for stable ELM-y H-mode operation with constant plasma parameters and sufficient pre-ELM measurements to produce pedestal profiles. A database of 261 pedestal profiles were produced over a range of auxiliary heating powers, plasma currents, top triangularities (δ_T), nitrogen seeding and deuterium fuelling rates as shown in Fig. 2. The NBH heating powers presented are defined as the power entering the main plasma chamber.

Fig. 2 was used to determine regions of high data density and comparable discharges prior to and after the upgrades. Scenarios with a plasma current of 170 kA and NBH of 800–900 kW entering the main plasma chamber were identified as the most routinely operated and thus the analysis will be primarily restricted to these. This scenario has previously been shown to produce type-I ELMs through a reduction in ELM frequency with decreasing auxiliary heating power [8]. There are a limited number of discharges with ECRH and this is due to the poor coupling in beam heated H-mode plasmas, resulting in large uncertainties in absorbed power. Therefore, the relatively few discharges with ECRH are omitted from this analysis. Fuelling rates of up to 10^{21} e/s and nitrogen seeding rates up to 10^{20} e/s were applied

during the discharges. For simplicity, fuelling and seeding rates will be categorised as outlined in Table 1.

3.1. Core, pedestal and divertor performance

Core performance was evaluated using the ITERH-98(y,2) scaling criteria and is shown as a function of divertor pressure and ELM averaged total radiated energy in Fig. 3A and B. The colours represent baffled (red) and unbaffled (black) discharges, with the symbol shape indicating the fuelling rate and the symbol size representing the nitrogen seeding rate. The entire range of δ_T and outer divertor targets (R_t) is included in this figure. A decrease in ITERH-98(y,2) with increasing divertor pressure was measured for both divertor configurations but a weaker decrease was measured after the baffled divertor upgrade. Discharges after the upgrade were also able to produce 2-3× higher total radiated energy at ITERH-98(y,2) greater than 1, providing clear evidence of increased performance.

Pedestal performance as a function of divertor pressure and line averaged density is presented in Fig. 3C and D. The highest P_{ped} achieved before and after the divertor upgrade was comparable. Discharges after the baffled divertor upgrade were able to maintain pedestal performance at 2-3× higher divertor neutral pressures. The pedestal pressure decreased with increasing line averaged density, implying the pedestal stability is limited by the ballooning boundary, as previously shown in [8].

Coupling of NBH with the plasma was estimated through ASTRA modelling [20]. Modelling of a subset of discharges indicated divertor neutral pressure and the baffled divertor upgrade did not systematically alter the coupled NBH power. A representative set of six discharges with approximately 500 kW of coupled NBH power at varying P_{ped} and divertor pressures is indicated by green arrows in Fig. 3C. Experiments are currently being conducted in the open divertor configuration to validate this.

The pedestal top T_e and n_e for a range of divertor pressures are presented in Fig. 4. Prior to the divertor upgrade, a decrease in pedestal top T_e was observed with increasing divertor pressure. Discharges after the divertor upgrade show pedestal top T_e being maintained across a range of divertor pressures. The pedestal top n_e is shown to vary by ±25% with no clear trend across the range of divertor pressures, indicating pedestal fuelling is likely saturated at low divertor pressures. The degradation of energy confinement and T_e with increasing divertor neutral indicates that core energy transport is stiff but particle transport is not.

The influence of δ_T and R_t on stored energy and P_{ped} is presented in Fig. 5. Discharges after the divertor upgrade produced generally higher ITERH-98(y,2) and P_{ped} across the range of δ_T. No trends between ITERH-98(y,2) and δ_T, P_{ped} or R_t were observed. A weak declining trend in maximum achievable P_{ped} was found with increasing δ_T Fig. 5 (middle) and its cause has not yet been identified. It can be concluded from the large variation in P_{ped} for a given δ_T or R_t that the influence of shaping is significantly lower than that of the divertor pressure or baffled divertor upgrade.

3.2. Influence of fuelling and seeding rates

Degradation of the H-mode pedestal with high fuelling and nitrogen seeding rates has previously been reported on TCV with an open divertor and the extended results of this work, shown in Fig. 6, support that finding [8]. The discharges after the baffled divertor upgrade showed lower P_{ped} degradation at fuelling and seeding up to 10^{20} e/s, after which a sharp decrease in P_{ped} was observed. The $Z_{eff.}$ was inferred by a fitting formula based on numerical simulations using neoclassical codes, as prescribed by the Sauter bootstrap current model [21,22]. This approach uses the experimentally measured Thomson Scattering profiles and loop voltage. It was observed to generally decrease at medium and high fuelling rates (◇ and + symbols). Post upgrade discharges produced an almost constant $Z_{eff.}$ with increasing divertor pressure, indicating significantly reduced neutral particle interaction with the core.

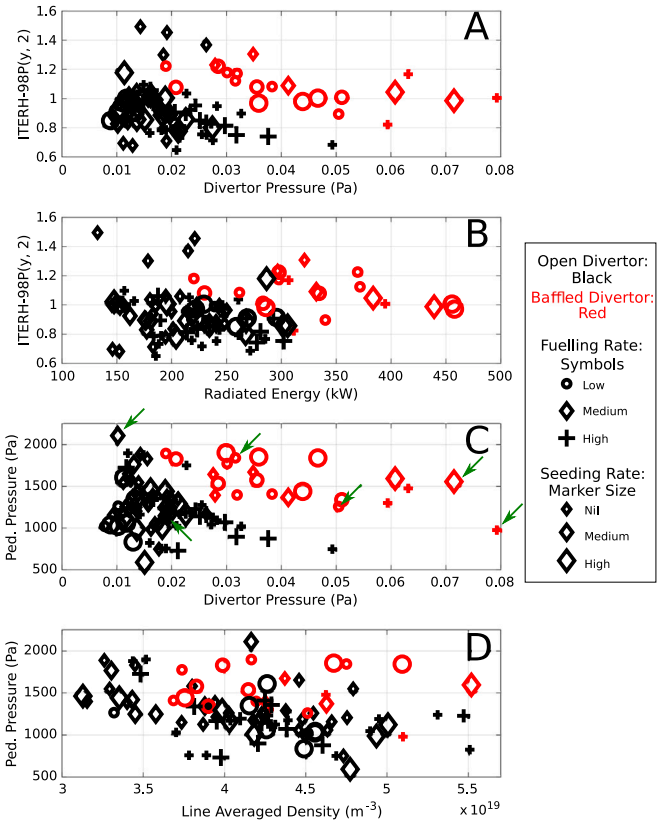

Fig. 3. ITERH-98(y,2) as function of divertor pressure (A) and ELM averaged total radiated energy (B), P_{ped} as a function of divertor pressure (C) and line average density (D). Green arrows in (C) indicate discharges with the same NBH power coupled to the plasma. (For interpretation of the references to colour in this figure legend, the reader is referred to the web version of this article.)

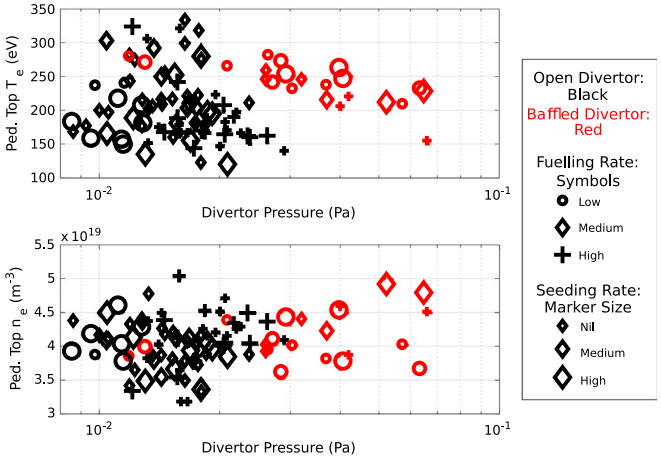

Fig. 4. Pedestal top T_e (top) and n_e (bottom) with divertor neutral pressure.

3.3. Pedestal structure

An outward shift in the n_e pedestal location, has been shown to reduce P_{ped} [5]. Fig. 7 presents the P_{ped} as a function of the T_e pedestal position, n_e pedestal position and the relative difference between the two. The pedestal position is defined by the location of the maximum gradient and a negative value in the relative position indicates the n_e pedestal is further out than the T_e pedestal. A decrease in P_{ped} was measured as the T_e and n_e pedestal positions moved outward prior to and after the baffled divertor upgrade (Fig. 7A and B). The T_e

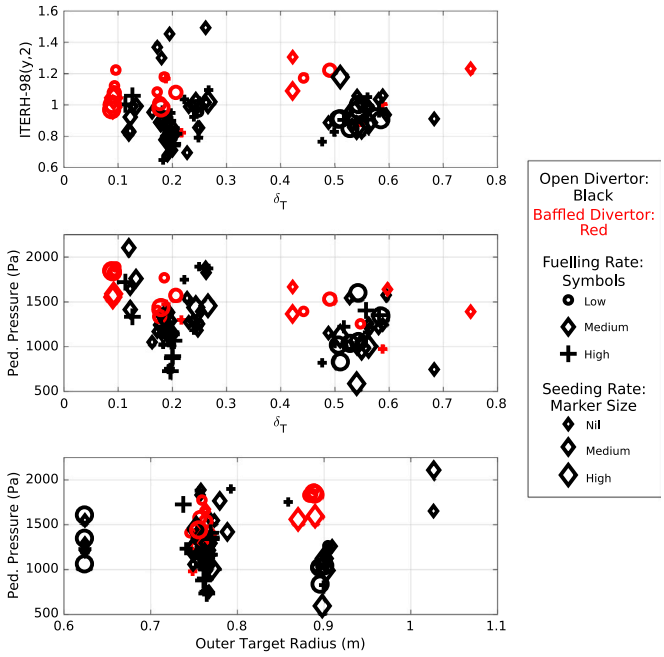

Fig. 5. ITERH-90(y,2) (top) and P_{ped} (middle) with δ_T. P_{ped} as a function of R_t (bottom).

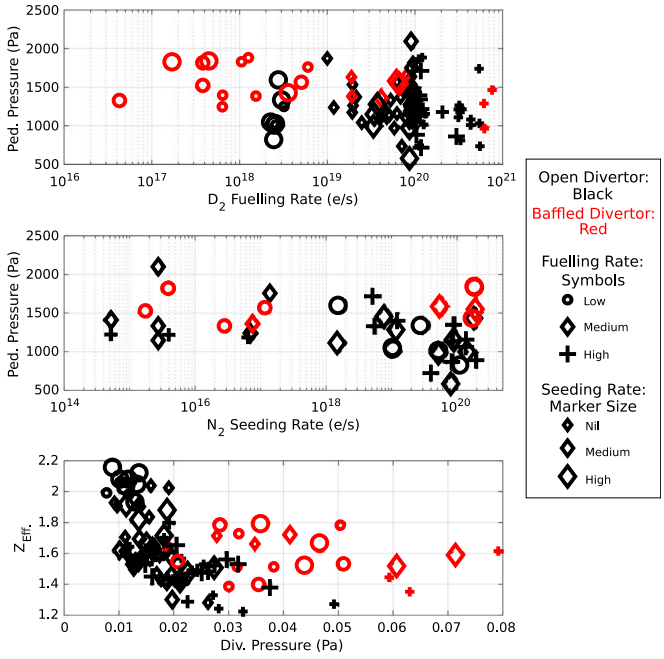

Fig. 6. P_{ped} at varying fuelling (top) and nitrogen seeding (middle) rates. $Z_{eff.}$ as a function of divertor pressure (bottom).

declined sharply outside ψ_N of 0.98 and n_e decreased steadily as the n_e pedestal position moved beyond ψ_N of 0.96. The outward shift of the n_e pedestal leading to a degradation in P_{ped} has also been observed AUG and JET [5,6]. The relative outward movement of the two positions does not produce a clear trend in P_e (Fig. 7C). The seperatrix density (n_{e-Sep}) was observed to strongly correlate with the outward shift of the n_e pedestal position (Fig. 7D).

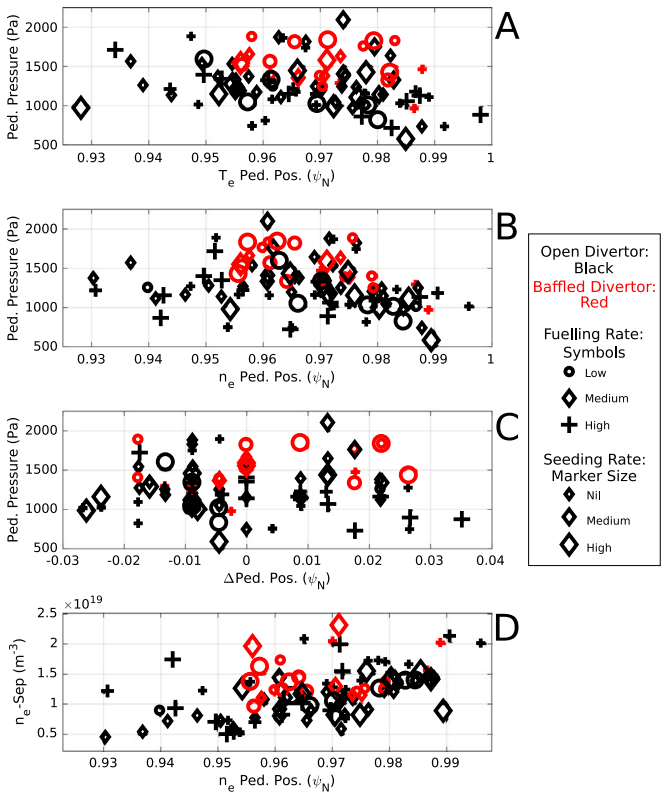

Fig. 7. Pedestal top pressure variation with T_e pedestal position (A), n_e pedestal position (B) and difference in T_e and n_e pedestal positions (C). n_{e-Sep} as a function of n_e pedestal position (D).

4. Stability analysis

A stability analysis was conducted on ~45 discharges to determine if the pedestal was on the critical boundary. The input parameters were the experimental equilibria, stored energies and measured T_e and n_e profiles. Ion temperatures (T_i) were assumed to be equal to T_e in the pedestal region and varied in the core to match the total stored energy. This assumption was validate as the electron stored energy was approximately half of the total stored energy for these discharges. Previous Z_{eff} scans between 1 and 3 resulted in a variation of P_{ped} of 15% and thus this analysis used a constant value of 2 for simplicity [8]. The pedestal density was fixed while the T_e and T_i gradients were scaled at constant width to produce a line of pedestal heights. The current density profiles were constrained with bootstrap current inferred from the Sauter model [21,22]. High resolution equilibria were then calculated using the HELENA code and the stability boundary was calculated using MISHKA for toroidal mode numbers between 1 and 40 [23,24]. The critical P_{ped} could then be calculated using the experimental pedestal width.

Fig. 8 presents the ratio of the experimental P_{ped} to the critical P_{ped} as a function of $\beta_\theta^{Ped.}$ (top), δ_T (middle) and Z_{eff} (bottom). The discharges at 170 kA with 800–900 kW of NBH are shown as bright symbols with the remaining dataset shown in faded symbols. The dashed horizontal lines indicate a ±25% variation between the critical P_{ped} and the measured P_{ped}. The bulk of the dataset is found to lie within these values and suggests the pedestals analysed in this study are close to the stability boundary. No systematic difference was found after the baffled divertor upgrade and no correlation between distance from the stability boundary and the P_{ped}, $\beta_\theta^{Ped.}$, δ_T, n_{e-Sep}, Z_{eff}, pedestal position or divertor pressure was observed.

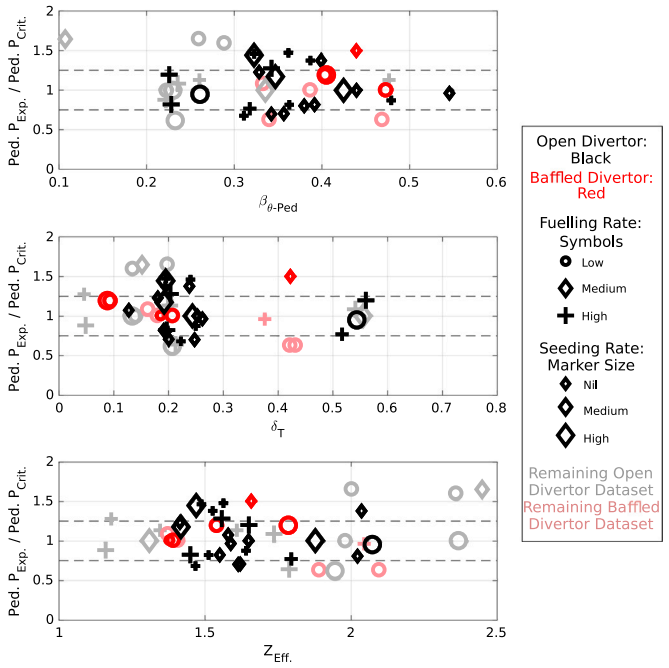

Fig. 8. Ratio of experimental pedestal pressure and critical pedestal pressure with pedestal β_θ (top), δ_T (middle) and Z_{eff} (bottom). Faded symbols indicate the database not selected in experimental analysis. The dashed lines indicate a ratio of ±0.25.

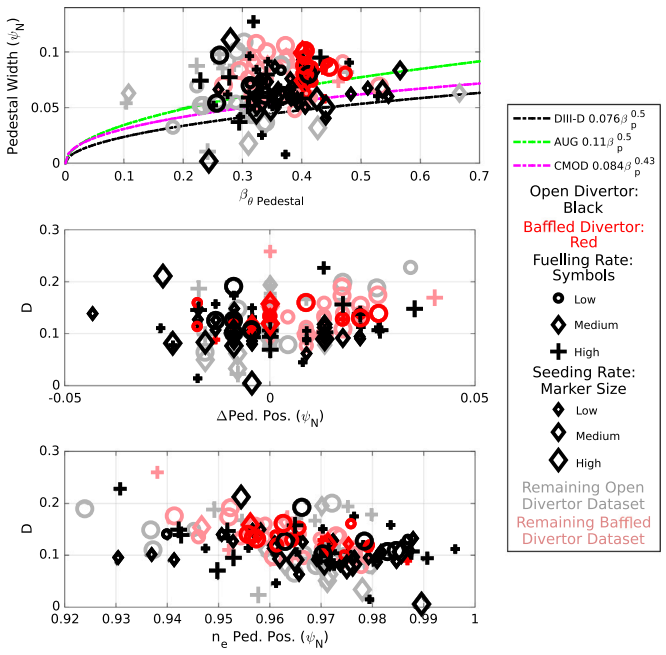

Fig. 9. Pedestal width as function of $\beta_\theta^{Ped.}$ (top). Relations observed on DIII-D, AUG and CMOD indicated with dashed lines. D with relative pedestal position (middle) and n_e pedestal position (bottom). Faded symbols indicate the remaining database not selected in the detailed analysis.

5. Comparisons with modelling

The correlation between pedestal width and $\beta_\theta^{Ped.}$ is presented in Fig. 9 (top). The fits from DIII-D, AUG and CMOD are overlaid for comparison [10]. Previously reported TCV data was shown to not lie on any one single fit and the D variable was found to vary from 0.05 to 0.13 [8]. The baffled divertor upgrade and inclusion of additional discharges present a similar result: TCV discharges do not follow the EPED1 approximation and the value of D varies between 0.02 and 0.3. This is in-line with results reported on JET where D was found to vary between 0.05 and 0.2 [6]. The bright baffled dataset (170 kA with 800–900 kW of NBH power) has an almost constant $\beta_\theta^{Ped.}$ with a factor of two variation in pedestal width. This strongly indicates that as transport increases, the gradient flattens and the width increases to maintain the same $\beta_\theta^{Ped.}$ at a different value of D.

The difference between TCV measurements and the EPED1 model predictions were previously partly attributed to relative changes in the T_e and n_e pedestal positions, which are not accounted for by the model [8]. Fig. 9 (middle) indicates that the inferred value of D does not correlate with the relative positions of T_e and n_e pedestals. Fig. 9 (bottom) suggests a weak decrease in D with an outward shift in the density pedestal position, indicating a reduction in cross-field transport as the density pedestal moves outward. No clear difference was observed between the baffled and unbaffled cases and transport simulations investigating the effect of neutrals on the plasma edge and the pedestal using the SolEdge2D-EIRENE code are still on-going [25, 26].

6. Conclusion

A database of ELM-y H-mode discharges prior to and after the baffled divertor upgrade has been examined. Discharges with 170 kA plasma current and 800–900 kW of NBH at varying fuelling and nitrogen seeding rates were the primary focus. It was found that P_{ped} was maintained after the baffled divertor upgrade at higher divertor pressures; a P_{ped} of 1.5 kPa was maintained at up to 4× higher divertor neutral pressures, resulting in up to 3× higher total radiated energy without ITERH-98(y,2) degradation. This result was shown to be consistent with changing δ_T and R_t. ASTRA modelling indicated the upgraded NBH optics did not systematically increase the coupled NBH power. These results indicate the baffled divertor upgrade has improved divertor performance whilst maintaining core performance.

Analysis of the pedestal structure showed a clear reduction in P_{ped} with an outward shift in n_e pedestal position for all discharges. The baffled divertor upgrade reduced the outward shift at high divertor neutral pressures and was thus able to maintain higher P_{ped}. Stability analysis of ~45 discharges showed that the bulk of these discharges were within 25% of the stability boundary. No correlation between the distance from the pedestal stability boundary and P_{ped}, $\beta_\theta^{Ped.}$, δ_T, n_{e-Sep}, Z_{eff}, pedestal position, divertor pressure or the baffled divertor upgrade was found.

Comparison with the EPED1 model indicated that TCV, like JET, does not follow the scaling between pedestal width and $\beta_\theta^{Ped.}$ reported on DIII-D, AUG and CMOD. The relating variable, D, was found to be constant on other machines but fluctuated in this study between 0.02 and 0.3. A factor of two variation in pedestal width for the same $\beta_\theta^{Ped.}$ was observed in baffled discharges at 170 kA with 800–900 kW of NBH. The difference between P_{ped} measurements and EPED1 model predictions was previously partially attributed to a relative shift in the T_e and n_e pedestal positions. The variation in D did not correlate with a relative shift in pedestal position but decreased with an outward shift of the density pedestal. The baffled divertor upgrade did not result in a systematic difference in D, the model parameter related to transport.

CRediT authorship contribution statement

U.A. Sheikh: Experiments, analysis, writing. **M. Dunne:** Experiments, analysis, modelling. **L. Frassinetti:** Experiments, analysis, methodology. **B. Labit:** Experiments, analysis. **P. Blanchard:** Experiments, analysis. **B.P. Duval:** Experiments, analysis. **O. Février:** Experiments, analysis. **D. Galassi:** Modelling. **A. Merle:** Modelling. **H. Reimerdes:** Experiments, analysis. **C. Theiler:** Experiments, analysis. **the TCV Team:** Experiments. **the EUROfusion MST1 Team:** Funding.

Declaration of competing interest

The authors declare that they have no known competing financial interests or personal relationships that could have appeared to influence the work reported in this paper.

Acknowledgements

This work has been carried out within the framework of the EUROfusion Consortium and has received funding from the Euratom research and training programme 2014–2018 and 2019–2020 under grant agreement No 633053. The views and opinions expressed herein do not necessarily reflect those of the European Commission. This work was supported in part by the Swiss National Science Foundation, Switzerland.

References

[1] F. Wagner, Plasma Phys. Control. Fusion 49 (2007) 12B.
[2] J.E. Kinsey, et al., Nucl. Fusion 51 (2011) 83001.
[3] S. Potzel, et al., J. Nucl. Mater. 463 (2015) 541.
[4] F. Reimold, et al., Nucl. Mater. Energy 12 (2017) 193.
[5] M.G. Dunne, et al., Plasma Phys. Control Fusion 59 (2017) 014017.
[6] L. Frassinetti, et al., Plasma Phys. Control. Fusion 59 (2017) 014014.
[7] E. Stefanikova, et al., Nucl. Fusion 58 (2018) 056010.
[8] U.A. Sheikh, et al., Plasma Phys. Control Fusion 61 (2019) 014002.
[9] L. Frassinetti, et al., Nucl. Fusion 59 (7) (2019) 076038.
[10] P. Snyder, et al., Plasma Phys. Control Fusion 45 (2003) 167.
[11] H. Reimerdes, et al., Nucl. Mater. Energy 12 (2017) 1106–1111.
[12] A. Fasoli, et al., Nucl. Fusion 60 (1) (2019) 016019.
[13] O. Février, et al., Nucl. Mater. Energy (2020) submitted for publication.
[14] H. Reimerdes, et al., Nucl. Fusion 61 (2) (2021) 024002.
[15] P. Blanchard, et al., Proc. 19th Laser Aided Plasma Diagnostic, J. Instrum. 14 (2019) C10038.
[16] R.J. Groebner, et al., Nucl. Fusion 41 (2001) 121789.
[17] L. Frassinetti, et al., Nucl. Fusion 61 (1) (2020) 016001.
[18] C.S. Pitcher, P.C. Stangeby, Plasma Phys. Control. Fusion 39 (1997) 779–930.
[19] S. Coda, et al., Nucl. Fusion 59 (2019) 112023.
[20] G.V. Pereverzev, et al., Max-Planck-Institut Für Plasma Physik, Rep. IPP 5142, 1991.
[21] O. Sauter, et al., Plasma Phys. Control Fusion 6 (1999) 7.
[22] O. Sauter, et al., Plasma Phys. Control Fusion 9 (2002) 12.
[23] C. Konz, et al., Proc. 38th EPS, 2011, p. 2.
[24] Mikhailovskii A.B., et al., Plasma Phys. Rep. 23 (1997) 713.
[25] H. Bufferand, et al., Nucl. Fusion 55 (5) (2015) 053025.
[26] D. Reiter, et al., Nucl. Mater. 196–198 (Supplement C) (1992) 80–89.